NRIAG JOURNAL OF ASTRONOMY AND GEOPHYSICS
2025, VOL. 14, NO. 1, 80–91
https://doi.org/10.1080/20909977.2025.2457299

Applying integrated geophysical methods to investigate groundwater seepage flow paths in the city of Jodhpur

Birendra Pratap

Department of Geophysics, Institute of Science, Banaras Hindu University, Varanasi, India

ABSTRACT

Anomalous seepage and groundwater accumulation in the basements of shops and houses in Jodhpur City, Rajasthan, are weakening foundations and reducing the lifespan of buildings due to damp walls and erosion. Therefore, identifying favourable fractured zones for groundwater seepage becomes crucial in this area. To investigate groundwater seepage flow paths, integrated geophysical surveys were conducted using self-potential (SP), geo-electrical resistivity, and very-low-frequency (VLF-EM) electromagnetic methods. Seventy-one vertical electrical soundings (VES) were carried out, along with three SP and three VLF profile lines using the Schlumberger array arrangement. The SP anomalies indicate groundwater flow through fractured formations. Geoelectrical and VLF cross-sections revealed the presence of fractured and semi-fractured rhyolite at depths ranging from 10 to 45 metres. The integrated results demonstrate that groundwater seepage flow paths are influenced by joints, cracks, and fractured zones, serving as conduits for groundwater flow in the study area.

ARTICLE HISTORY
Received 7 August 2023
Revised 9 January 2025
Accepted 18 January 2025

KEYWORDS
Flow paths; groundwater; seepage; self-potential; very-low frequency

1. Introduction

A global image of the groundwater seepage problem was difficult to obtain using conventional methods due to their expensive, time-consuming, and limited coverage (Abidin et al. 2015). These limitations have created gaps in determining the most suitable method that can fulfill several considerations related to cost, time and result quality. Compared to using a single geophysical method alone, an integrated approach usually provides more reliable information (Vargemezis et al. 2012; Ojo et al. 2015; Shishaye et al. 2019). In recent years, integrated geophysical method has been increasingly adopted in many studies related to water seepage and environmental problems. Additionally, it has made a useful contribution in identifying subsurface features, such as cavities, faults, fractures, and other structures, that cause the majority of water seepage from reservoirs and dams (Idornigie and Olorunfemi 2010; Al-Fares 2011; Dailey et al. 2015).

A large number of groundwater problems associated with exploration and exploitation could be investigated using geophysical methods (Oladunjoye et al. 2013; Nyam et al. 2014; Arifianto et al. 2018). These methods can also be used to study structural controls that affect groundwater flow and accumulation (Abraham et al. 2013; Dailey et al. 2015). Self-potential and electrical resistivity measurements are used to investigate seepage at a remote moraine dam in the Sierra Nevada of California (Moore et al. 2011). In Syria, integrated geophysical approaches, including electromagnetic (EM), electrical sounding (ES), and electrical resistivity tomography (ERT), were used to understand the water loss problem at the Afamia B dam in the Al-Ghab basin (Al-Fares 2011). Similarly, an Electrical Resistivity Tomography (ERT) survey was conducted at the Abu Baara earth dam in northwestern Syria to identify leakage pathways near the dam body (Al-Fares 2014). In Southwestern Nigeria, integrated geophysical techniques involving very low frequency electromagnetic (VLF-EM), magnetic intensity, and electrical resistivity were used to investigate possible internal seepage at the University of Ilorin Dam in Kwara State (Olasunkanmi et al. 2018). Electrical resistivity and self-potential technologies are increasingly being used for seepage investigations and dam safety evaluations (Panthulu et al. 2001; Lim et al. 2004) and the time-lapse measurement technique further enhances their capability to detect seepage anomalies (Sjödahl et al. 2010).

A significant portion of India is currently experiencing a decline in the water table, but in some parts of Jodhpur city, there has been an unusual rise in groundwater levels, covering approximately 40% of the city's land area and expanding gradually. This has raised concerns due to its adverse effects on the region. The problem was visualised when subsoil water started oozing out in the underground structures of several shops in the city, leading to erosion, dampness, wall damage and instability in house

CONTACT Birendra Pratap bpratap@bhu.ac.in Department of Geophysics, Institute of Science, Banaras Hindu University, Varanasi 221005, India

foundations. Hydrogeological, hydrochemical, and isotopic studies have indicated that the water seepage in the city is primarily caused by the rising water level in Kailana Lake-Takht Sagar (Jigyasa 2011; Yadav and Pratap 2015; Kaur and Ramanathan 2016). Further research is required to investigate the groundwater seepage flow paths and characterise the fracture zones contributing to the seepage problem. Integrated geophysical methods were utilised to identify the groundwater seepage flow paths and fractured zones responsible for the seepage in the study area.

2. Description of the study area

The study area comprises parts of Jodhpur city and its adjoining area, covering about 172 km^2 geographically. It is situated in the western part of Rajasthan, lying between the latitudes 26° 13' N and 26° 20' N and the longitudes 72° 56' E and 73° 04' E. The study area falls under Survey of India toposheet numbers 45F/3, 45F/4, 45B/15, and 45B/16. The main part of the study area falls under the Luni and Mandor Blocks of Jodhpur district. Jodhpur district is bounded in the north by Bikaner, in the North West by Jaisalmer, in the east by Nagaur and Pali, in the south by Pali and Barmer, and in the west by Jaisalmer districts. Jodhpur town has a peculiar geomorphologic setting. The old walled city part is located on the hill slope area and at the base of the fort hill ridge. The sloping land gradually turns to plain alluvial terrain towards the south, east and southwest.

The city of Jodhpur has several traditional water impounding structures, such as baories, ponds, jhalaras, and open wells. The major surface water bodies namely Kailana Lake -Takht Sagar, are located in the west of the city and are well connected for water storage. These structures originally provided water for the city by collecting rainwater in their catchments. However, the population of Jodhpur has increased significantly in the past ten years, leading to a higher demand for water. Despite various water supply initiatives, the supply has not kept up with the demand. The Rajiv Gandhi Lift Canal (RGLC), continuously delivers water to Kailana Lake- Takht Sagar, and these water bodies have been expanded to accommodate the increased water storage needs. Unfortunately, unforeseen circumstances have caused seepage and water build-up in the underground basements of several residential and commercial properties in the city.

3. Geology and hydrogeology

The geological configuration of the Jodhpur district is characterised by the presence of the Trans-Aravalli (Marwar supergroup), the Malani suite (Chauhan et al. 1991; Dasgupta and Bulgauda 1994; Bhushan and Khullar 1998; Kochhar 1998) and the Vindhyan super group. Paliwal (1992) reported that the Malani bed consists of felsite and quartziferous porphyries. The geological formation of Jodhpur city and adjoining areas is mainly composed of sedimentary rocks like sandstone, shale, and limestone of the Vindhyan super-group, with certain areas occupied by the rhyolite suite (Blanford 1877; Paliwal 1992). These formations are highly deformed due to tectonic activities (GWD, 2001). It is believed that during these tectonic processes, some major lineaments developed and extended up to several kilometres towards the city area. The study area consists of a number of flat-topped hills of sandstone and rhyolite trending NE-SW direction.

In the city, geological formations like Malani rhyolite and Jodhpur sandstone are inter-layered with shales. The lower flow of Malani rhyolite is highly faulted, folded, weathered and fractured due to tectonic processes. Kailana Lake – Takht Sagar is also situated on this type of rock formation. The Jodhpur group of rocks, such as shale and sandstone, cover the maximum area of the old walled city. The shale and sandstone are deformed due to the Neotectonic activity of the area. It is assumed that the development of some major lineaments in terms of faults, joints and fractures, which extends towards the city area. A number of parallel joints trending NE-SW and E-W directions have also developed in rhyolite, shale and sandstone formations due to Neotectonic activity. The Jodhpur city and adjoining area comprise rocks of Upper Proterozoic to Lower Paleozoic age, i.e. Malani suite of igneous rocks and Jodhpur group of sedimentary rocks.

Groundwater in Malani rhyolites occurs under water table conditions and moves along the joints and fractures. It forms a poor aquifer due to the absence of porosity and permeability. However, in some places, it is highly weathered, fractured and jointed, which contain a good quantity of groundwater. Jodhpur sandstone forms an aquifer in the central northern and western parts of the study area. It is medium to fine-grained, hard, compact, and generally occurs with intercalations of shale, which reduces the water potential. Quaternary formations form an aquifer in the south, south east, and south west parts of the study area. It comprises older alluvium containing sand, silt, clay with kankar, transported material of sandstone and rhyolite (gravel and pebbles etc.) rock fragments. The south west part of the alluvium (hydrogeological formation) directly follows the grey and pink granites.

4. Material and geophysical methods

A comprehensive field survey, including self-potential, electrical resistivity and very-low frequency methods, was carried out to acquire data.

The self-potential (SP) method is a passive geophysical technique commonly used to characterise fluid flow through a porous medium (Boleve et al. 2007). In the earth, an electrical potential is generated from mineral bodies, geochemical reactions and groundwater movement by the process known as electrokinetic coupling (Perrier et al. 1998; Revil and Leroy 2001). The SP method measures, naturally occurring ground potentials on the ground surface and correlates them to seepage paths or changing groundwater flow patterns (Jardani et al. 2007; Richards et al. 2010). The SP method is extensively used in common hydrogeological problems, particularly in cases where dams and lakes suffer leakage through the bedrock, especially in earth-filled dams built over faulted and deformed structures (Panthulu et al. 2001; Song et al. 2005; Al-Fares 2011; Moore et al. 2011).

The SP measurement was taken using a fixed reference method, with 5 metres of potential electrode separation (Sirles 1997; Panthulu et al. 2001). The base station was selected at a convenient point for operation, where no significant variations in potential were observed. Noise issues related to electrodes were addressed by using special non-polarisable electrodes with a large contact area to minimise contact potential noise (Panthulu et al. 2001; Nwokebuihe et al. 2017). To ensure consistent readings, each station's hole was prepared in advance and watered 5–6 hours before measurements were taken. A resistivity metre (DDR-2) manufactured by IGIS, Hyderabad, India with a measuring accuracy of 0.1 mV, was used for conducting SP surveys. Three profile lines, X-X', Y-Y' and Z-Z' were conducted in the study area, each with a length of 500 metres. The profile X-X'ran nearly parallel to Kailana Lake-Takht Sagar, while Y-Y' and Z-Z' are parallel to X-X' with offset distances of 50 metres and 100 metres respectively, towards the geoelectrical cross-section E-E'. All SP profiles were oriented in a South-North direction, as depicted in Figure 1.

The geoelectrical resistivity method is primarily applied in geological mapping. It is used to obtain information concerning the subsurface geoelectrical layers and the location of water-saturated zones, their thickness, and depth (Aanuoluwa and Ayobami 2012; Ibrahim 2013). This method has been extensively used on dam sites for seepage investigation (Panthulu et al. 2001, Cho and Yeom, 2007; Sjödahl et al. 2010; Moore et al. 2011). Standard vertical electrical sounding (VES) surveys are used to detect and map the groundwater seepage zones (Titov et al. 2000; Johansson et al. 2002; Abidin et al. 2015). The resistivity anomaly varies depending on the nature of the seepage path or if seepage is not occurring along the survey line (Cho and Yeom, 2007; Kumar 2012). Fractured zones saturated with water and other weak zones generally produce low-resistivity anomalies due to serving as active seepage conduits or the presence of other weathered zones.

The geoelectrical sounding data were carried out using the Terrameter SAS 300 manufactured by M/s. ABEM Sweden, with the application of Schlumberger configuration with two sets of current electrode separations. A total of 71 geoelectrical sounding data were used, including some new and a few old data points.

The old sounding data were collected from the Groundwater Department, Jodhpur. The locations of geoelectrical soundings and cross-sections are shown in Figure 1. The values of apparent resistivity were plotted against the half-current electrode spacing on double logarithmic scale paper with a modulus of 62.5 mm. To interpret the field VES curves, two stages were undertaken: first, the layer parameters were manually interpreted using curve matching techniques, and then the data were processed and interpreted using software. This interpretation provides details on each layers resistivity and thickness. The results are useful for delineating geologic features and subsurface materials relevant to groundwater flow paths.

The VLF method is potentially useful for detecting long, straight electrical conductors, such as conductive faults and fracture zones, especially water-bearing fracture zones in hard rock areas (Sharma and Baranwal 2005; Sundararajan et al. 2007; Gurer et al. 2009; Vargemezis et al. 2012; Michael et al. 2013; Adelusi et al. 2014). The use of the VLF-EM technique, on the other hand, serves as a prospecting tool for quickly mapping near subsurface geological structures and the presence of fractures (Tijani et al. 2009; Revil et al. 2012; Aizebeokhai and Oyeyemi 2014). This method successfully measures the resistivity contrast at the boundaries of fractured zones with a high degree of connectivity. Recently, the very-low frequency method has been used for mapping water seepage zones from lakes/reservoirs (Khalil et al. 2009; Alexopoulos et al. 2011).

The ABEM-WADI VLF instrument was used for the VLF survey. The WADI has a memory to store about 4000 measurements. The data can be retrieved from the memory at any time. Moreover, the WADI can be connected to a printer or a computer for the interpretation of data. Eighteen VLF profiles were taken using frequencies 18.1, 19.1 19.8 and 27.5 kHz. The total length of each profile was 100 m. The observation interval was kept at 10 m to demarcate the depth and extent of the weathered and fractured zone. VLF profiles were taken along a line for the preparation of VLF sections and the orientation of all the VLF profiles is approximately in a south-north direction as shown in Figure 1.

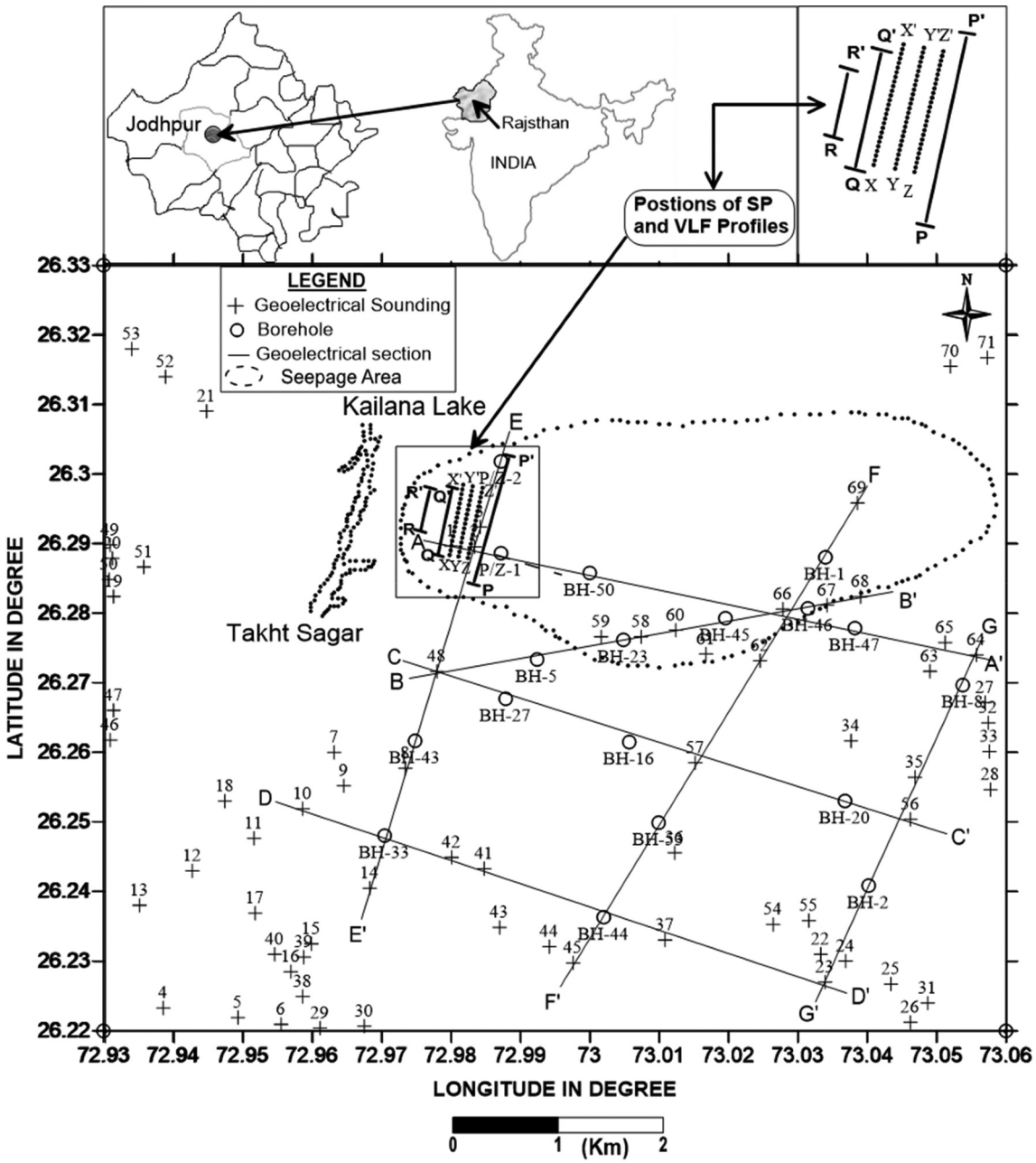

Figure 1. Location map showing geoelectrical cross sections, VLF profiles and SP profiles.

5. Results and discussions

5.1. Water table contour map

The depth of water the table was converted with reference to the mean sea level as a reference level (RL) of the water table. Contour maps of the RL of the water table have been prepared for the pre- and post-monsoon seasons for the entire study period. Out of these contour maps, only a few representative contour maps are presented and discussed. The pre-monsoon season and post-monsoon season contour maps have been prepared to show the hydraulic gradient of the area. Hence, two contour maps Figures 2a,b, were prepared using pre-monsoon and post-monsoon water table data for the same season to illustrate water flow in the study area and the impact of rainfall. Comparative studies of these figures clearly indicate that the pattern of the contours is similar in nature with the highest water level in the north-east corner and the lowest in the south-east. Water flows from higher to lower altitudes on the water table, predominantly in the east and south-east directions, as shown in Figure 2.

In both figures, the highest water level is located in the northeast corner with a latitude range of 26.28° to 26.32° and a longitude range of 72.94° to 72.96°. The lowest contour value is 170 m for both seasons and is centred in the southeast portion of the area with latitudes 26.25° to 26.27° and longitudes 73.00° to 73.05°. The flow of water starts from higher altitudes to lower altitude of water table RLs. In the study area, water flow is predominantly in two directions east and

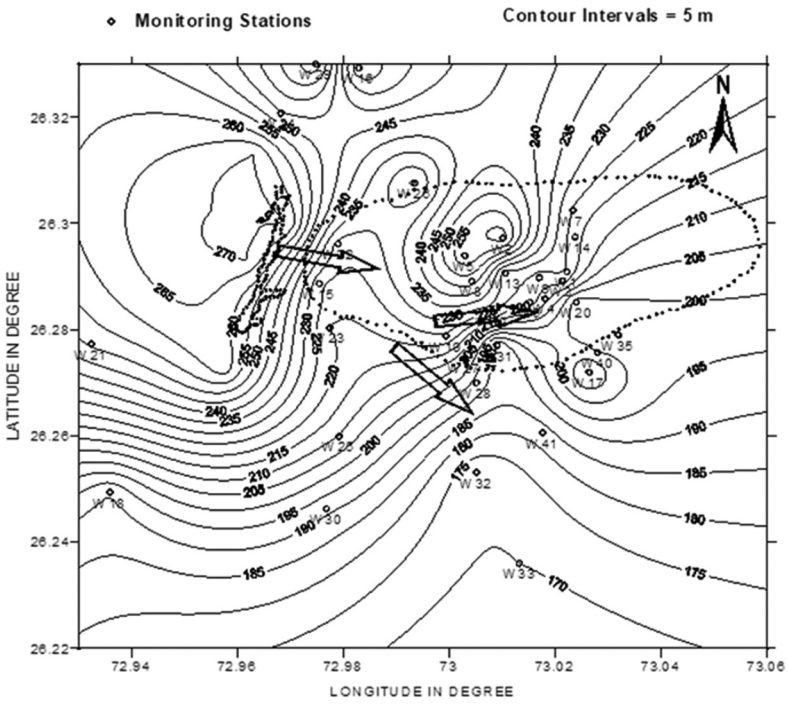

(a)

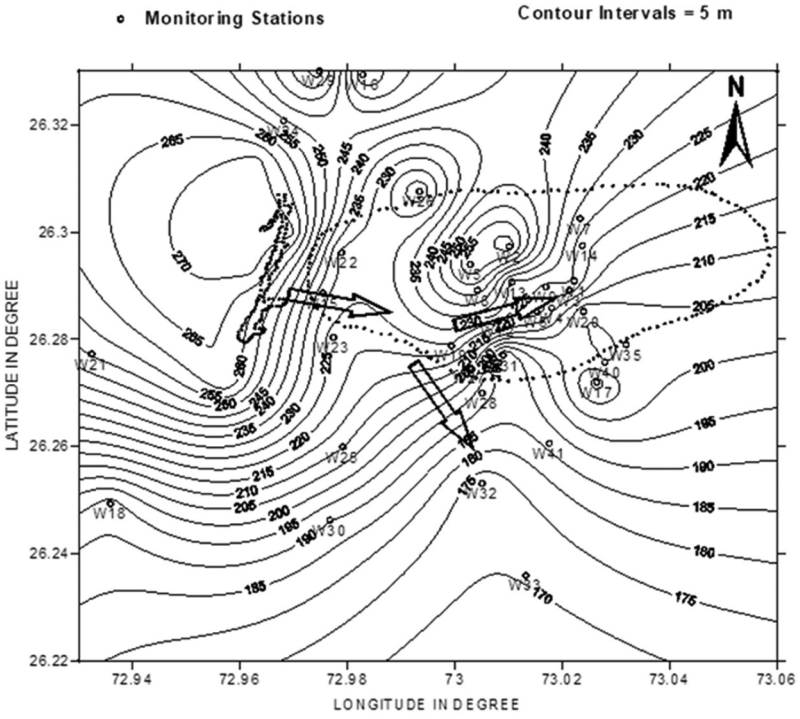

(b)

Figure 2. Contour map showing the direction of ground water flow (a) during pre-monsoon and (b) post-monsoon period.

southeast. However, the hydraulic gradient is steeper on the eastern side compared to the southeaster side.

5.2. Self-potential

The interpretation of SP data is mainly qualitative. The movement of groundwater in the formation affects the magnitude and sign (±) of SP. The SP values have been plotted against the distance of the measuring electrodes with reference to the base electrode. The observed positive SP anomaly is interpreted keeping in view that it is caused by a streaming potential, which is developed due to the flow of groundwater in the fractured formation (Schiavone and Quarto 1984; Moore et al. 2011). The results of the SP profiles are shown in Figure 3(a–c). The profile X-X' displayed positive SP anomalies identified as AX1, AX2, AX3, and A×4ranging in value from 7.6 mV to 16.5 mV. The largest values of the SP anomaly at A×1and A×4indicated large seepage zones of groundwater

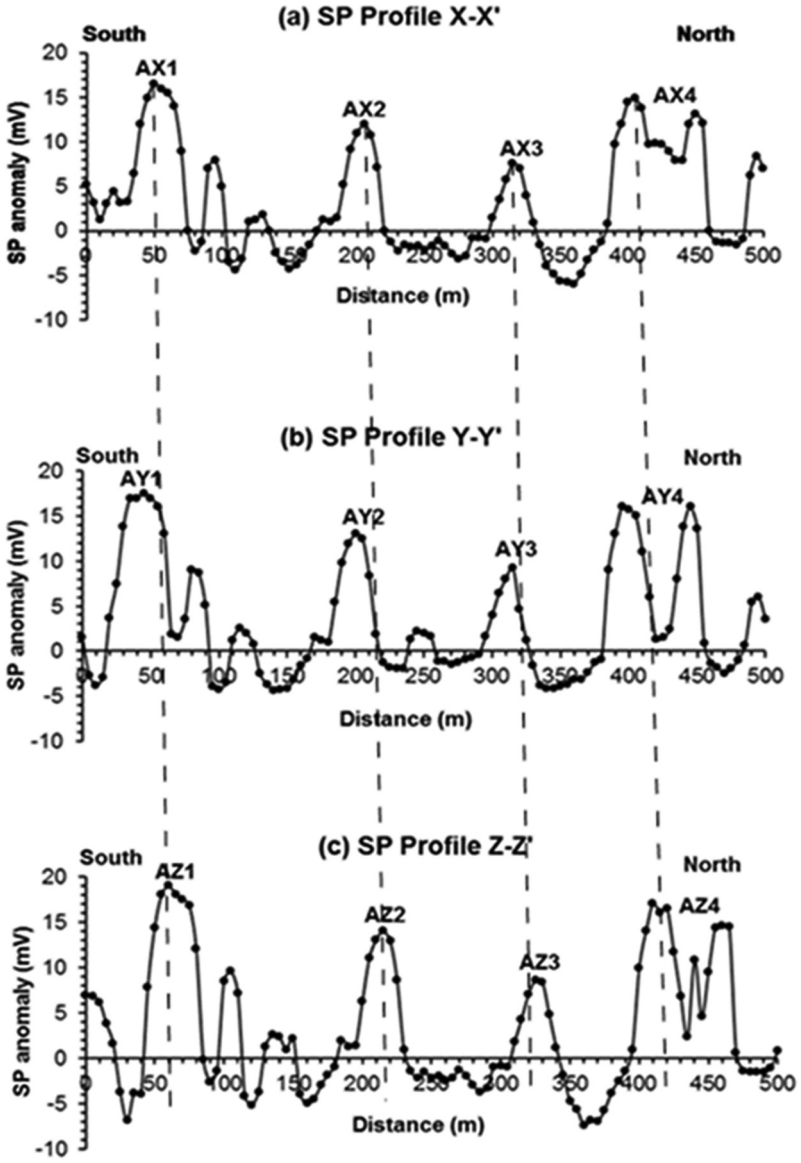

Figure 3. Response of self-potential anomalies (a) along profile X-X′ (b) along profile Y-Y′ and (c) along profile Z-Z′.

following routes. The profile Y-Y' exhibited similar behaviour, with AY1, AY2, AY3, and AY4 showing the highest values of SP ranging from 8 mV to 17.5 mV, indicating larger seepage flow channels. Profile Z-Z' contained observable positive anomalies AZ1, AZ2, AZ3, and AZ4, with the anomaly ranging from 8.4 mV to 19 mV. The negative anomaly suggest infiltration of water from one path to another closest path (Oglivy et al. 1969; Al-Saigh et al. 1994).

The comparative analysis of Figure 3 shows that the highest SP anomalies are observed at A×1and A×4in profile X-X', AY1 and AY4 in profile Y-Y', and AZ1 and AZ4 in profile Z-Z', indicating the same groundwater seepage flow paths. The increase in positive SP anomaly from one profile to the next indicates the movement of seepage groundwater from profile X-X' to profile Z-Z'. Although the amplitude of the SP anomaly increases only slightly from one profile to the next, they are clearly connected, which is consistent with the contour map in Figure 4. Similar patterns are observed in the contour map, which align with positive SP profile peaks. The contour map's SP anomalies, which show the highest values at offsets of 50 m, 200 m, 310 m, 400 m, and 450 m, suggest the potential presence of seepage routes. These seepage channels correspond to the fractured zones identified by the geoelectrical cross-sections in Figures 5 and 7.

5.3. Geoelectrical resistivity

Based on the interpreted results of geoelectrical soundings and lithological data from boreholes, seven vertical geoelectrical sections were prepared. The sections deliver a clear picture of the subsurface formations and cracked zones that support the groundwater seepage flow routes. For ease of reference, only the geoelectrical sections covering the majority of the seepage region in the areas have been included.

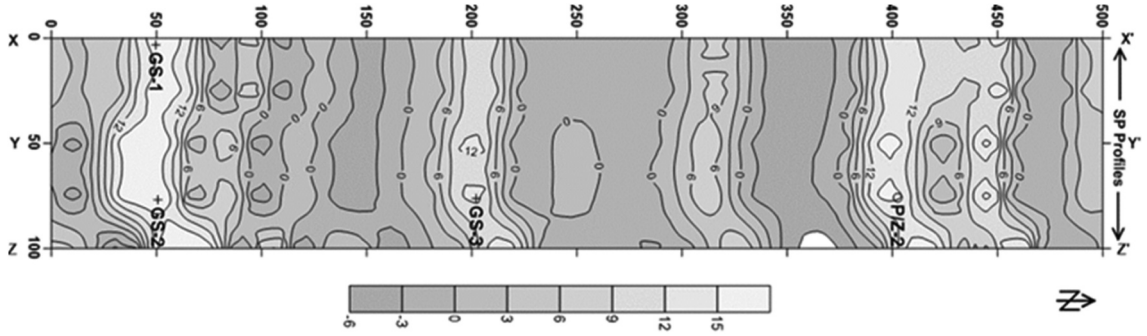

Figure 4. Contour map of SP anomaly of anomalous water seepage zones.

5.3.1. Geoelectrical section for profile A-A′

The section includes most of the area affected by seepage and spans 8 kilometres in a WNW-ESE direction as shown in Figure 5. The geoelectrical section was created using five geo-electrical soundings results, as well as data from the piezometer (P/z-1) and boreholes BH-50 and BH-47 for lithology correlation. With the exception of GS-65, which has five layers, the segment generally consists of four layers. The western end of the section passes through a seepage zone. The resistivity in the top layer ranges from 50 Ωm to 395 Ωm, indicating sand mixed with wind-blown sandy soil. Due to varying soil characteristics and moisture levels, the surface soil resistivity values vary by location. The top layer is 1–3 metres thick. The section describes various lithological/geological unit types, including semi-fractured rhyolite (resistivity 203–248 Ωm), fractured rhyolite (resistivity 50–110 Ωm), and compact rhyolite (resistivity 516–994 Ωm) on the western side. The section also contains sand with kankar (resistivity 57–70 Ωm), shale (resistivity 14–28 Ωm), sandstone (resistivity 127 Ωm), and very resistive rhyolite on the eastern side. The fractured zone has a resistivity range of 50 Ωm to 127 Ωm at GS-1, GS-2/3, and GS-65, located slightly above the bedrock. The upper part of the section on the western side covers semi-fractured to fractured rhyolite, with potential groundwater seepage in both horizontal and vertical directions.

5.3.2. Geoelectrical section for profile B-B′

Six geoelectrical soundings were used to create the 6.6 km long geo-electrical section B-B', oriented in the WSW-ENE direction as shown in Figure 6. To correlate the hydrogeological formation, lithological data from boreholes BH-5, BH-23, BH-45, and BH-46 were included. The resistivity of the surface layer ranges from 42 Ωm to 170 Ωm, with a thickness of 1 m to 4 m. The second layer consists of sand and kankar, with resistivity ranging from 40 Ωm to 120 Ωm. The lithological sequence on the western side includes fractured rhyolite (resistivity 125–210 Ωm) and semi-fractured rhyolite (resistivity 500 Ωm) from top to bottom. The remaining part of the segment consists of rhyolite (very resistant), shale (resistivity 20–25 Ωm), and sandstone (150 Ωm). Sand covers the upper part of the segment up to fractured rhyolite on the western side to enhance groundwater flow routes.

5.3.3. Geoelectrical section for profile E-E′

This section was created using the lithology of piezometer P/z-2, boreholes BH-43 and BH-33, and the results of four geoelectrical soundings, as shown in Figure 7. The section runs in the NNE-SSW direction for a total length of 7.4 km. A four-layer stratification is observed over the entire geo-electric cross-section.

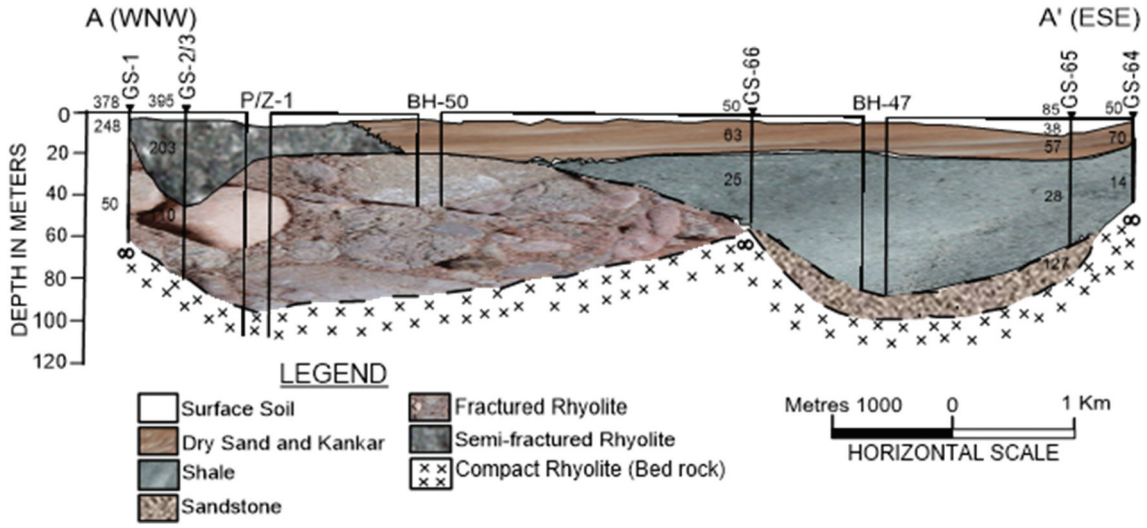

Figure 5. Geoelectrical section along profile A-A′.

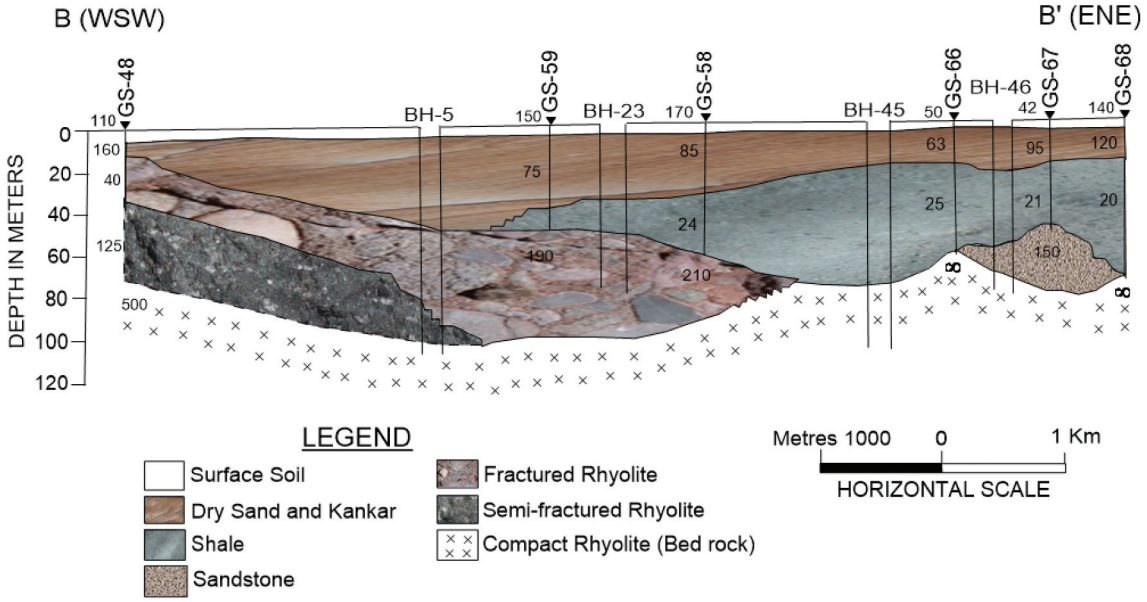

Figure 6. Geoelectrical section along profile B-B′.

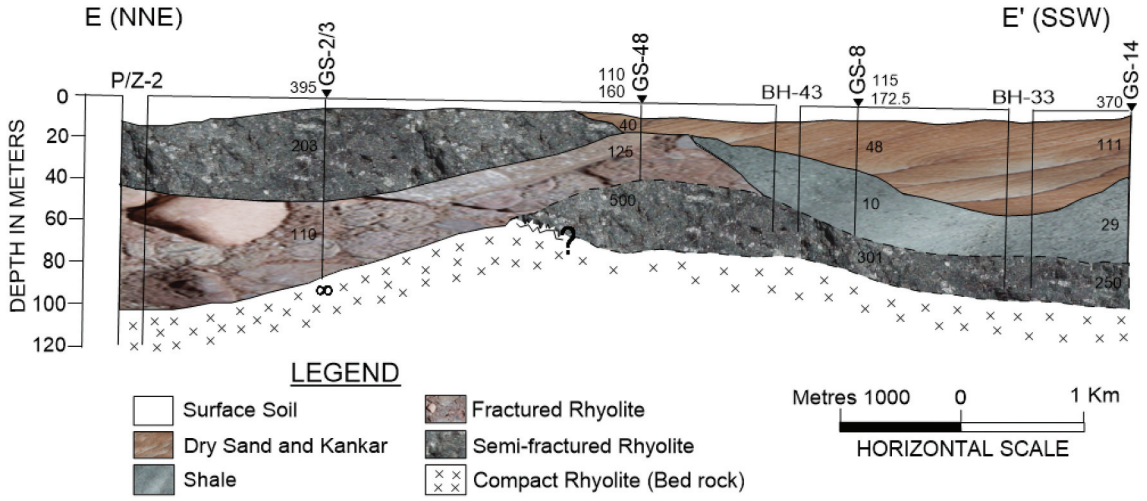

Figure 7. Geoelectrical section along profile E-E′.

The top layer is composed of surface soil with resistivity between 110 and 395 Ωm and a thickness ranging from 1 to 5 m. On the southern side, resistivity ranges from 40 to 111 Ωm, indicating the presence of dry sand with kankar. The second layer is filled with partially cracked rhyolite with a resistivity of 203 Ωm on the northern side. The third geo-electric layer consists of fractured rhyolite on the northern side (resistivity 110–125 Ωm) and a thick layer of shale between BH-43 and GS-14 on the southern side (resistivity 10–29 Ωm). Near the middle of the section, both formations are compressed. The remaining portion reflects the existence of semi-fractured rhyolite, and the last layer represents the bedrock on the northern side of the section.

5.3.4. Geoelectrical section for profile F-F′

Figure 8 displays a geoelectrical section created using five geo-electrical soundings, as well as data from the boreholes BH-1, BH-53, and BH-44 for lithology correlation. The section spans 8.8 kilometres in a NE-SW direction. The surface soil has a resistivity ranging from 40 Ωm to 180 Ωm, with a thickness of 1–6 m and is stratified into four layers. The second layer contains dry sand and kankar with resistivity ranging from 34 Ωm to 93 Ωm and a thickness of 8–32 metres. The third layer, with a resistivity of 10 Ωm to 26 Ωm, consists of shale with sandstone in the middle, and has a thickness of 32–48 metres. The final layer includes rhyolite covered by granite on the southern side, semi-fractured rhyolite in the middle, and compact rhyolite on the northern

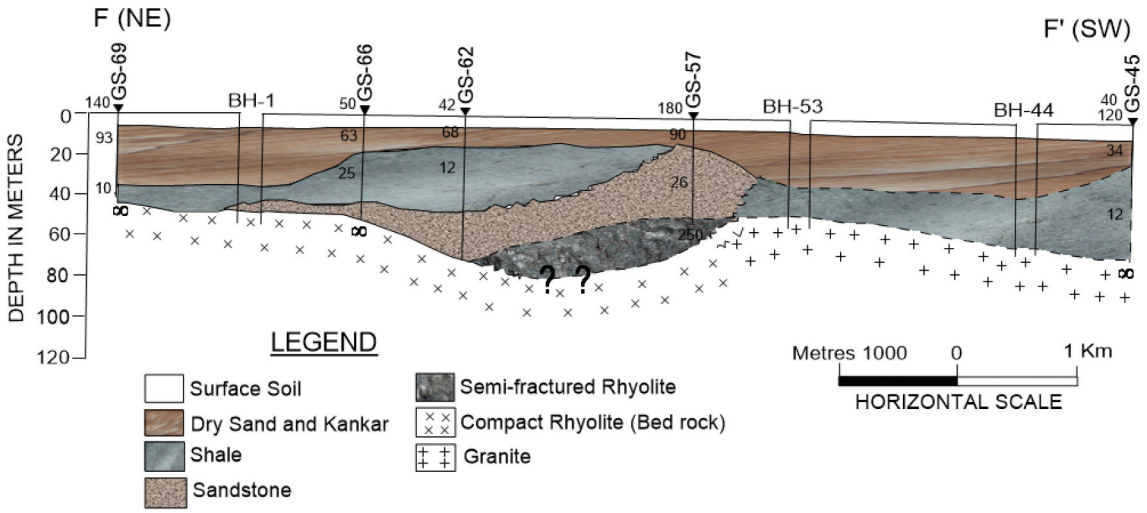

Figure 8. Geoelectrical section along profile F-F′.

side. The top slice of the section contains sand, sandstone, and/or shale sedimentary strata with minor bedrock fissures and fractures, which support the groundwater seepage paths.

5.4. Very-low frequency electromagnetic

In this study, filtered data were used to prepare VLF sections, which were then interpreted using the SECTOR program. Based on the interpretation of the 18 VLF profiles, three vertical VLF sections (P-P', Q-Q', and R-R') were prepared to delineate the presence of fractured zones, their depth, and areal coverage (Sinha, 1990; Ogilvy and Lee, 1991).

5.4.1. VLF section P-P′

The VLF section P-P' was created using interpreted results from seven VLF profiles, each 100 m in length with 10 m observation intervals. This section spans 700 m from south to north, as depicted in Figure 9. The section indicates the presence of weathered and fractured rocks starting at a depth of 10 m, likely continuing to a depth of 45 m. An isolated weathered pocket is found at approximately 5 m depth, with a variable thickness of 5–9 m. The section clearly shows multiple weathered and fractured rock bodies at various depths. Many locations have weathered formations just beneath the soil layer, which extends to a depth of 50 m. The VLF section reveals that weathered and fractured rocks cover the entire area to a depth of more than 50 m.

5.4.2. VLF section Q-Q′

The interpreted results from five VLF profiles were used to create the VLF section Q-Q'. Each profile was 100 metres long with observations taken at 10-m intervals. The VLF section Q-Q' is located 50 m to the east of the P-P' profile and runs in a south-north direction, covering a total length of 500 metres as shown in Figure 10. The section reveals that weathering typically begins at the surface and extends to depths of over 50 m. Additionally, there are numerous isolated patches of weathered or fractured zones that extend up to 20 m below the surface. The section clearly indicates that over 50% of the area is occupied by weathered or fractured rocks, which act as conduits for groundwater seepage flow paths.

5.4.3. VLF section R-R′

The VLF section R-R' was prepared based on the interpretation of three VLF profiles, each 100 m in length with 10 m observation intervals. This section runs from south to north near Kailana Lake-Thkhat Sager and is only 300 m long, as shown in Figure 11. Further observations

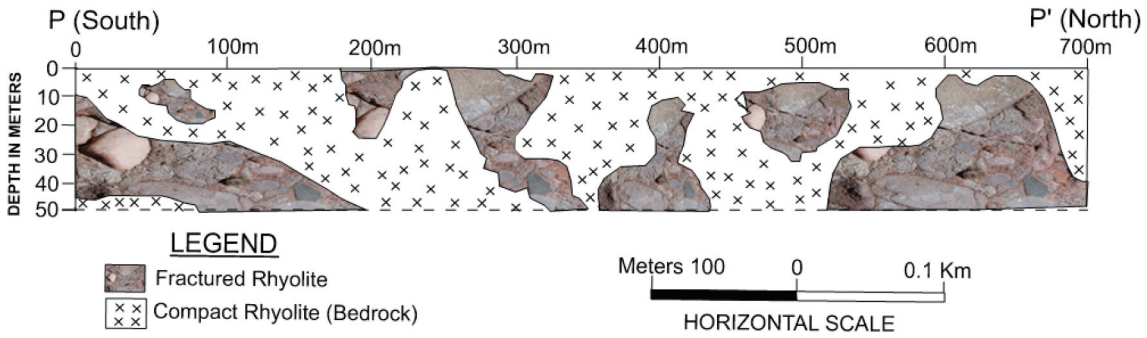

Figure 9. VLF section along profile PP′.

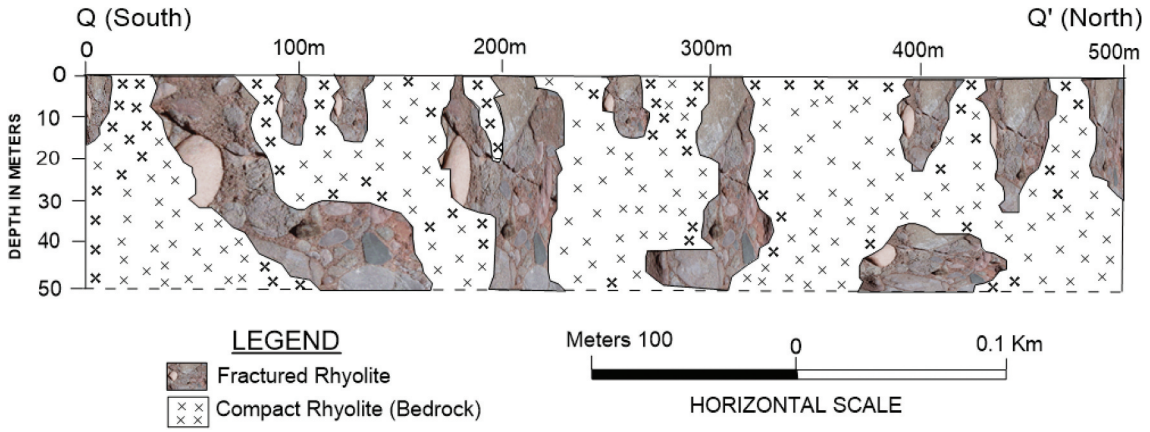

Figure 10. VLF section along profile QQ′.

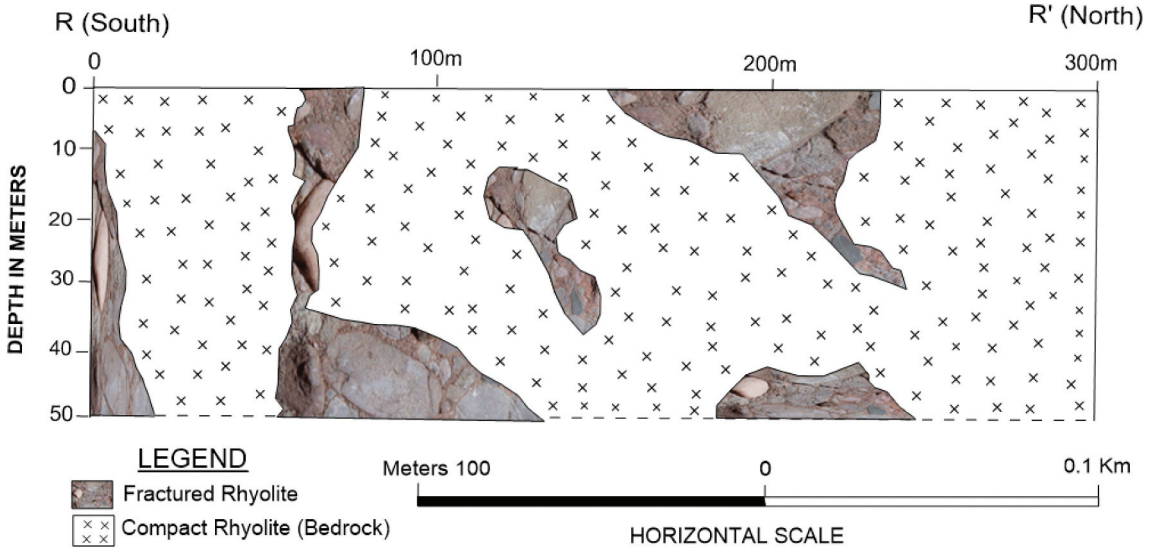

Figure 11. VLF section along profile RR′.

were not possible due to a lack of suitable open space. The section indicates a narrow fracture zone located at a shallow depth, extending more than 50 m. It also delineates the dipping nature of the fractured zone in the southern direction, supporting groundwater seepage flow paths.

6. Conclusion

The analysis of the integrated results reveals numerous shear joints and bedding joints in the foundation rock of the study area, which are weathered, semi-fractured, and fractured due to tectonic activity. The analysis of SP data indicates seepage flow activities with the greatest intensity at offsets of 50, 200, 310, 400, and 450 metres. Geo-electrical cross-sections show cracked zones parallel to seepage channels, with prevalent rhyolites from the surface to greater depths. Weathered formations are found both near the surface and at greater depths, with weathered and fractured zones likely extending up to 45 metres as indicated in VLF sections. An isolated weathered rock pocket of rhyolites is present at a depth of 5 metres, with a variable thickness of 5–19 m. The overall lithology and areal distribution of fractured zones, present at different depth levels throughout the study area advocate the seepage of groundwater. These formations increase the rate of water seepage through interconnected fractured zones from Kailana Lake-Takht Sagar towards the city and its adjoining area.

The research paper provides new insights into the relationship between groundwater and surface water, groundwater flow paths, and mapping of seepage zones. Future research plans include constructing a cluster of boreholes at a suitable site to pump excess water from the city, and divert it to water deficit areas for irrigation, industrial, and other purposes. Furthermore, cement grouting of the bottom and walls of reservoirs can be employed to prevent underground water flow and safeguard underground structures, building foundations, and shops in the Jodhpur city.

Acknowledgments

The author would like to express gratitude to the Department of Geophysics, Institute of Science, Banaras Hindu University, Varanasi, for providing the necessary facilities for this research. Additionally, the author is thankful to the Chief Engineer and former Head of Geophysics Wing, Ground Water Department, Jodhpur, Rajasthan, for granting permission to access and share data, as well as for the facilities provided during fieldwork.

Disclosure statement

No potential conflict of interest was reported by the author(s).

Funding

The author(s) reported there is no funding associated with the work featured in this article.

ORCID

Birendra Pratap http://orcid.org/0000-0002-7059-4516

Author contributions

Authors have contributed to writing the manuscript, acquisition and interpretation of data, and drawing the figures.

Availability of data and material

The datasets used and/or analysed during the study are available from the corresponding author upon reasonable request.

References

Aanuoluwa AT, Ayobami SL. 2012. Geoelectric assessment of groundwater prospect and vulnerability of overburden aquifers at Adumasun area, Oniye, Southwestern Nigeria. Archiv Appl Sci Res. 4(5):2077–2093.

Abidin MHZ, Baharuddin MFT, Zawawi MH, Ali NM, Madun A, Ahmad Tajudin SA. 2015. Groundwater seepage mapping using electrical resistivity imaging. Appl Mech Mater. 773-774:1524–1534. doi: 10.4028/www.scientific.net/AMM.773-774.1524.

Abraham B, Yirgale G, Gebrehiwot G. 2013. Application of vertical electrical sounding and horizontal profiling methods to decipher the existing subsurface stratification in River Segen Dam Site, Tigray, Northern Ethiopia. J Environ Earth Sci. 3(10):42–54.

Adelusi AO, Ayuk MA, Kayode JS. 2014. VLF-EM and VES: an application to groundwater exploration in a Precambrian basement terrain SW Nigeria. Ann Geophys. 57(1):1–11. doi: 10.4401/ag-6291.

Aizebeokhai PA, Oyeyemi KD. 2014. Application of geoelectrical resistivity imaging and VLF-EM for subsurface characterization in a sedimentary terrain, Southwestern Nigeria. Arab J Geosci. 8(6):4083–4099. doi: 10.1007/s12517-014-1482-z.

Alexopoulos JD, Dilalos S, Vassilakis E. 2011. Adumbration of amvrakia's spring water pathways, based on detailed geophysical data (Kastraki -Meteora). In: Advances in the research of aquatic environment. Vol. 2. Berlin Heidelberg: © Springer-Verlag. doi: 10.1007/978-3-642-24076-8.

Al-Fares W. 2011. Contribution of the geophysical methods in characterizing the water leakage in afamia B dam, Syria. J Appl Geophys. 75(3):464–471. doi: 10.1016/j.jappgeo.2011.07.014.

Al-Fares W. 2014. Application of electrical resistivity tomography technique for characterizing leakage problem in Abu Baara Earth Dam, Syria. Int J Geophys. 2014:1–9. doi: 10.1155/2014/368128.

Al-Saigh NH, Mohammed ZS, Dahham MS. 1994. Detection of water leakage from dams by self-potential method. Eng Geol. 37(2):115–121. doi: 10.1016/0013-7952(94)90046-9.

Arifianto I, Savitri KP, Priana MRF, Setianto A. 2018. Groundwater exploration in volcanic morphology using geophysical schlumberger resistivity method. Jeneponto, South Sulawesi Province. Proceedings of the 13th SEGJ International Symposium,Yokyo 2018; South Sulawesi Province, Indonesia.

Bhushan SK, Khullar VK. 1998. Geochemistry and tectonic significance of dyke swarm in malani igneous complex around Sankara, district Jaisalmer, Rajasthan. In: Paliwal BS, editor. The Indian Precambrian. (India), Jodhpur: Scientific Publishers; p. 482–491.

Blanford WT. 1877. Geological notes on the great Indian desert between Sind and Rajasthan.Rec. Geol Surv India. 10(1):1–54.

Boleve A, Crespy A, Revil A, Janod F, Mattiuzzo JL. 2007. Streaming potentials of granular media: influence of the Dukhin and Reynolds numbers. J Geophys Res. 112: B08204. doi: 10.1029/2006JB004673.

Chauhan DS, Dubey JC, Ram B. 1991. Geological analysis of part of Nagaur basin in the vicinity of Jodhpur city. In: Tandon SK, Pant CC Casshyap SM, editors. Sedimentary basin of India. Nanital India: Gyanodaya Prakashan; p. 64–73.

Dailey D, Saucka W, Sultana M, Milewskib A, Ahmeda M, Latond WR, Elkadiria R, Fosterd J, Schmidta C, Al Harbia T. 2015. Geophysical, remote sensing, GIS, and isotopic applications for a better understanding of the structural controls on groundwater flow in the Mojave Desert, California. J Hydrol: Reg Stud. 3:211–232. doi: 10.1016/j.ejrh.2014.12.002.

Dasgupta V, Bulgauda SS. 1994. An overview of the geology and hydrocarbon occurrences in western part of Bikaner-Nagaur basin Indi. J Petrol Geol. 3(1):1–17.

Gurer A, Bayrak M, Gurer OF. 2009. A VLF survey using current gathering phenomena for tracing buried faults of Fethiye–Burdur Fault Zone, Turkey. J Appl Geophys. 68 (3):437–447. doi: 10.1016/j.jappgeo.2009.03.011.

GWD. 2001. Rising water level problem in Jodhpur City area Rajasthan. State Unit Office Jodhpur.

Ibrahim E. 2013. Geoelectric resistivity survey for site investigation in east Matruh area, north western desert, Egypt. World Appl Sci J. 21(7):008–1016. doi: 10.5829/idosi.wasj.2013.21.7.2871.

Idornigie AI, Olorunfemi O. 2010. A geoelectric mapping of the basement structures of the south-central part of the bida basin and its hydrogeological implications. J Min Geol. 28:93–103.

Jardani A, Revil A, Boleve A, Dupont JP, Barrash W, Malama B. 2007. Tomography of groundwater flow from self-potential (SP) data. Geophys Res Lett. 34(24): L24403. doi: 10.1029/2007GL031907.

Jigyasa S. 2011. Seasonal variation in ground water quality of Jodhpur city and surrounding areas. Res J Chem Environ. 5:883–888.

Johansson S, Dahlin T, Friborg J. 2002. Seepage monitoring by resistivity and streaming potential measurements at Hällby embankment dam 1996–1999. Report 00:15. Stockholm: Elforsk. 47.

Kaur L, Ramanathan AL. 2016. Assessment of major ion chemistry in ground water and surface water of Kailana Lake Area of Jodhpur (Rajasthan). JoWREM. 3(2):42–56.

Khalil MA, Monteiro Santos FA, Moustafa SM, Saad UM. 2009. Mapping water seepage from Lake Nasser, Egypt, using the VLF-EM method: a case study. J Geophys Eng. 6(2):101–110. doi: 10.1088/1742-2132/6/2/001.

Kochhar N. 1998. Malani igneous suite of rocks. J Geol Soc India. 51:120.

Kumar D. 2012. Efficacy of electrical resistivity tomography technique in mapping shallow subsurface anomaly. J Geol Soc India. 80(3):304–307. doi: 10.1007/s12594-012-0148-2.

Lim HD, Kim KS, Kim JH, Kwon HS, Oh BH. 2004. Leakage detection of earth dam using geophysical methods. Proceedings of the 72th Annual Meeting of International Commission on Large Dams (ICOLD) p. 212–224; Seoul, Korea.

Michael O, Moruffdeen A, Onil A. 2013. Groundwater prospecting and exploration in a low potential hard rock aquifer: case study from Ogbomoso North, Southwestern Nigeria. J Environ Earth Sci. 3(14):84–102.

Moore JR, Boleve A, Sanders JW, Glaser SD. 2011. Self-potential investigation of moraine dam seepage. J Appl Geophys. 74 (4):277–286. doi: 10.1016/j.jappgeo.2011.06.014.

Nwokebuihe, Chinedu S. 2017. The use of geophysical methods for dam seepage investigations and dredged oyster deposit characterization. Doctoral dissertations. http://scholarsmine.mst.edu/doctoraldissertations/2567.

Nyam FMEA, Mbarga TN, Nouck PN, Assembe S, Dicoum EM. 2014. Ground water exploration using geoelectrical investigation in Bafia Area, Cameroon. J Earth Sci Geotech Eng. 4(3):61–75.

Ogilvy RD, Lee AC 1991. Interpretation of VLF–EM inphase data using current density pseudosections. Geophys. Prospect. 39:567–580.

Oglivy AA, Ayed MA, Bogoslovsky VA. 1969. Geophysical studies for water leakages from reservoirs. Geophys Prospect. 17(1):36–62. doi: 10.1111/j.1365-2478.1969.tb02071.x .

Ojo JS, Olorunfemi MO, Akintorinwa OJ, Bayode S, Omosuyi GO, Akinluyi FO. 2015. GIS integrated geomorphological, geological and geoelectrical assessment of the groundwater potential of akure metropolis, Southwest Nigeria. J Earth Sci Geotech Eng. 5(14):85–101.

Oladunjoye HT, Odunaike RK, Ogunsola P, Olaleye OA. 2013. Evaluation of groundwater potential using electrical resistivity method in Okenugbo area, Ago -Iwoye, Southwestern Nigeria. Int J Eng Appl Sci. 4(5):225–232.

Olasunkanmi NK, Aina A, Olatunji S, Bawala M. 2018. Seepage investigation on an existing dam using integrated geophysical methods. J Environ Earth Sci. 8(5):6–16.

Paliwal BS. 1992. Tectonics of the post-Aravalli mountain building activity and its bearing on the accumulation of sediments along the western flank of the Aravalli range, rajathan, India. In: Ahmed R, and Sheikh AM, editors. Geology in the South Asia-I Proc. of GEOSAS-I Islamabad, Pakistan, Feb. 23-27, 1992. Hydrocarbon Development Institute of Pakistan, 1994; p. 52–60. Jodhpur(India): Scientific Publishers.

Panthulu TV, Krishnaiah C, Shirke JM. 2001. Detection of seepage paths in earth dams using self-potential and electrical resistivity methods. Eng Geol. 59(3–4):281–295. doi: 10.1016/S0013-7952(00)00082-X.

Perrier F, Trique M, Lorne B, Avouch JP, Auto S, Tarits P. 1998. Electrical variation associated with yearly lake level variations. Geophys Res Lett. 25(11):1955–1958. doi: 10.1029/98GL01139.

Revil A, Karaoulis M, Johnson T, Kemna AA. 2012. Revisão: Alguns métodos elétricos de baixa frequência para a caraterização da subsuperfície e monitorização em hidrogeologia. Hydrogeol J. 20(4):617–658. doi: 10.1007/s10040-011-0819-x.

Revil A, Leroy P. 2001. Hydroelectric coupling in a clayey material. Geophys Res Lett. 28(8):1643–1646. doi: 10.1029/2000GL012268.

Richards R, Revil A, Jardani A, Henderson F, Batzle M, Haas A. 2010. Pattern of shallow ground water flow at Mount Princeton Hot Springs, Colorado, using geoelectrical methods. J Volcanol Geotherm Res. 198 (2010):217–232. doi: 10.1016/j.jvolgeores.2010.09.001.

Schiavone D, Quarto R. 1984. Self-potential prospecting in the study of water movements. Geoexploration. 22 (1):47–58. doi: 10.1016/0016-7142(84)90005-X.

Sharma SP, Baranwal VC. 2005. Delineation of groundwater-bearing fracture zones in a hard rock area integrating very low frequency electromagnetic and resistivity data. J Appl Geophys. 57(2):155–166. doi: 10.1016/j.jappgeo.2004.10.003.

Shishaye HA, Tait DR, Befus KM, Damien T, Maher DT. 2019. Uma abordagem integrada para caracterização de aquífero e avaliação da produtividade de água subterrânea na bacia do Lago Haramaya, Etiópia. Hydrogeol J. 27 (6):2121–2136. doi: 10.1007/s10040-019-01956-7.

Sinha AK 1990. Interpretation of ground VLF-EM data in terms of vertical conductor models. Geoexploration. 26:213–231.

Sirles P. 1997. Seepage investigation using geophysical techniques at Coursier Lake Dam, B. C. Canada. Symposium of the Geophysical Application to Environmental and Engineering Problems (SAGGEP); Reno-(NV). 1. p. 321–331.

Sjödahl P, Dahlin T, Johansson S. 2010. Using the resistivity method for leakage detection in a blind test at the Røssvatn embankment dam test facility in Norway. Bull Eng Geol Environ. 69(4):643–658. doi: 10.1007/s10064-010-0314-y.

Song SH, Song Y, Kwon BD. 2005. Application of hydrogeological and geophysical methods to delineate leakage pathways in an earth fill dam. Exploration Geophysics. 36 (1):92–96. doi: 10.1071/EG05092.

Sundararajan NG, Nandakumar MN, Srinivas Y. 2007. VES and VLF—an application to groundwater exploration, Khammam, India. Lead Edge. 26(6):708–716. doi: 10.1190/1.2748489.

Tijani MN, Osinowo OO, Ogedengbe O. 2009. Mapping subsurface fracture systems using integrated electrical resistivity profiling and VLF–EM methods: a case study of suspected gold mineralization. RMZ Mater Geoenviron. 56(4):415–436.

Titov K, Loukhmanov V, Potapov A. 2000. Monitoring of water seepage from a reservoir using resistivity and self-polarization methods: case history of the petergoph fountain water supply system. First Break. 18 (10):431–435. doi: 10.1046/j.1365-2397.2000.00096.x.

Vargemezis G, Tsourlos P, Stampolidis A. 2012. A focusing approach to ground water detection by means of electrical and EM methods, the case of Paliouri, Northern Greece. Stud Geophys Geod. 56(4):1063–1078. doi: 10.1007/s11200-011-0444-0.

Yadav GS, Pratap B. 2015. Identification of responsible source for rise in ground water table of Jodhpur City, Rajasthan, India. Int J Earthquake Engg GeolSci. 5(1):1–14.